European Polymer Journal 72 (2015) 238–255

Contents lists available at ScienceDirect

European Polymer Journal

journal homepage: www.elsevier.com/locate/europolj

Macromolecular Nanotechnology

The orientation-enhancing effect of diphenyl aluminium phosphate nanorods in a liquid-crystalline epoxy matrix ordered by magnetic field

Beata Mossety-Leszczak [a,*], Beata Strachota [b], Adam Strachota [b], Miloš Steinhart [b], Miroslav Šlouf [b]

[a] Department of Industrial and Materials Chemistry, Rzeszów University of Technology, Al. Powstańców Warszawy 12, 35-959 Rzeszów, Poland
[b] Institute of Macromolecular Chemistry v.v.i., Academy of Sciences of the Czech Republic, Heyrovskeho nam. 2, CZ-162 00 Praha, Czech Republic

ARTICLE INFO

Article history:
Received 23 July 2015
Received in revised form 18 September 2015
Accepted 21 September 2015
Available online 25 September 2015

Keywords:
Liquid-crystalline epoxy resins
Magnetic field orientation
Nanocomposites
Nanorods

ABSTRACT

Nano-crystallites of diphenyl aluminium phosphate (NR), the polymeric molecules of which display a nanorod-like shape, were incorporated as an orientation-enhancing agent into an epoxy matrix, which was obtained by the cure of a liquid crystalline diepoxide containing a triaromatic mesogenic group. The crosslinking component of the matrix was 4,4′-diaminodiphenylmethane. Samples of the neat matrix and of the composite with NR were oriented by applying an external magnetic field during their cure. The cure process was investigated by DSC and in-situ rheology, and the obtained products were characterised by TEM, 1D- and 2D-SAXS/WAXS, DSC and DMTA. It was demonstrated, that the cuboid but anisotropic NR crystallites become oriented and highly enhance the ordering of the liquid crystalline matrix in the magnetic field. Some spontaneous ordering by NR was observed even without any field. The ordering effect of the field was stronger if it was perpendicular to, rather than parallel with the main surface of the flat samples. The dynamic-mechanical properties of the products displayed the expected anisotropy, while their thermal transitions were found to be sensitive to the achieved degree of ordering.

1. Introduction

Epoxy resins are an important thermoset class, as well as a popular matrix in advanced composites. They have a wide application field, e.g. in composites for the aviation industry, or in electronics as encapsulation or coating materials, or as glues [1]. Of key importance for the mentioned applications are the epoxies' good thermal, mechanical and dielectric properties, their resistance to corrosion and low shrinkage upon cure. Their properties can be further improved by incorporation of co-monomers or additives, which enhance the epoxies' thermal stability, adhesion to various surfaces, toughness, flexibility, corrosion resistance or which introduce new properties like flame retardancy or electrical conductivity.

An advanced method of epoxy resins modification is the introduction of rigid mesogenic groups into their network. These building blocks can improve the resin's mechanical properties and reduce its brittleness. The simplest way of preparing this kind of networks is the crosslinking of neat liquid crystalline epoxy monomers (LCEM). The crosslinking can be achieved

* Corresponding author.
E-mail addresses: mossety@prz.rzeszow.pl (B. Mossety-Leszczak), beata@imc.cas.cz (B. Strachota), strachota@imc.cas.cz (A. Strachota), steinhart@imc.cas.cz (M. Steinhart), slouf@imc.cas.cz (M. Šlouf).

http://dx.doi.org/10.1016/j.eurpolymj.2015.09.018
0014-3057/

thermally (epoxy homo-polymerisation), chemically (e.g. with suitable amines) or photochemically, and if it is carried out at a sufficiently low temperature it yields crosslinked solids with a preserved liquid crystalline order. In the recent years, the synthesis of numerous novel LCEM has been reported, and their liquid crystallinity and cure behaviour has been investigated [2,3]. The attractive properties of liquid crystalline thermosets (LCT) are given by the retention of the liquid crystalline phase structure and of its orientation throughout the cure process. The ordering alters the thermal conductivity of the LCTs, as well as their mechanical and optical properties. The LCT's morphology and their degree of order strictly depend on the cure conditions. Liquid crystalline monomers can form an isotropic or liquid crystalline phase structure, monodomain or polydomain, depending on the chosen cure temperature. LCTs cured in the absence a force field typically display a polydomain liquid crystalline structure. In a recent work [4] it was demonstrated, that the fracture toughness even of a polydomain LCT was higher than in case of its isotropic-cured analogue and that the difference became more distinct with the enlargement of the domain diameter in the ordered LCT sample.

LCTs with oriented monodomain structure are of great interest due to their high and anisotropic mechanical properties, and also because their optical anisotropy could be of use in nonlinear optics and in photoreactive materials [5,6]. Several methods have been employed to induce the macroscopic alignment of mesogenic molecules of LCT precursors. Oriented epoxy LCTs have been prepared by curing mesogenic diepoxides in a magnetic [5,7,8] or electric [9] field, or in a glass test cell containing a substrate with a special surface pattern made of rubbed polyimide layers [10] (epitaxy). A similar case like the last example is the reported macroscopic orientation of liquid crystalline epoxies which was spontaneously induced by cure on a carbon fibre (CF) surface [11,12] (orientation along the long molecular axis of CF). A similar result was also obtained with oriented multi-walled carbon nanotubes [13]. The macroscopic orientation enhanced the moduli as well as the thermal stability of the carbon-LC-epoxy composites [11–13].

Among the tested methods, the ordering of LCT precursors with a strong magnetic field is the most popular one [5–7,14–17], due to several advantages it offers. The high-strength magnetic field remains relatively constant throughout the crosslinking process, it causes an orientation of mesogens in the entire sample and it is easier and safer to work with than strong electric field. The magnetic-field-method yielded systems with the order parameter of around 0.38–0.48 [18], 0.5–0.6 [14], 0.65 [6], 0.71 [19,20], 0.8 [21], or above 0.84 [22], if primary aromatic diamines were used as a curing agents.

The principle of the ordering effect of the magnetic field is illustrated in the Scheme 1. A detailed explanation of this phenomenon, which considers the shape anisotropy, is given in [23] and [24]. Typical organic molecules (without radicals or transition metal atoms which have unpaired electrons) are diamagnetic. Diamagnetic materials react to an applied magnetic field by an induced field of opposite direction. Consequently, the magnetic field in the diamagnetic material is weakened (the field lines are partly expelled, see Scheme 1a). As consequence of this interaction, diamagnetic materials are expelled from strong magnetic fields. Rod-like 'normal' molecules can be considered as pieces of diamagnetic material. At a constant volume fraction, the arrangement of rod-like molecules parallel to the field lines makes possible the diamagnetic interaction on a smaller cross-section, than in case of rods arranged perpendicularly to the field (see Scheme 1b vs. Scheme 1c). Hence, the parallel-ordered state has a lower energy and is preferred. Additionally, an eventual anisotropy of the magnetic susceptibility of rod-like molecules further enhances their ordering in the magnetic field [23,24].

Distinct effects of the macroscopic orientation by the magnetic field on the epoxies' properties (see Scheme 2) and on the anisotropy of these properties were observed in the above cited works. In comparison to analogous samples cured without the magnetic field, the oriented LCTs display improved tensile moduli, break strength and elongation at break [5,21]. The fracture toughness in the direction perpendicular to the applied field increases dramatically [20,25]. In the direction of the orientation, the dynamic mechanical properties were enhanced (storage modulus increase) [5,7,16–18,20]. The thermal conductivity was found to display a significantly higher value in the orientation direction than in the perpendicular one [19]. The coefficient of thermal expansion (CTE) of the ordered networks is highly anisotropic. In the aligned networks, there is a substantial reduction in the CTE parallel to the direction of the magnetic field, if compared to their randomly oriented analogues, while the CTE perpendicular to the field direction increases as a function of orientation [7,14,16–18,20–22].

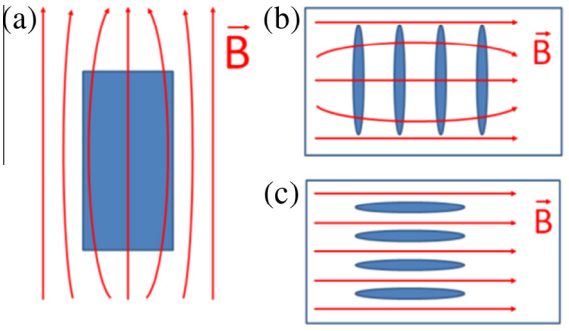

Scheme 1. Interaction of the magnetic field with a compact piece of diamagnetic material (a) and with rod-like diamagnetic molecules (b and c) the orientation of the molecules parallel to the field leads to a smaller amount of unfavourable interaction.

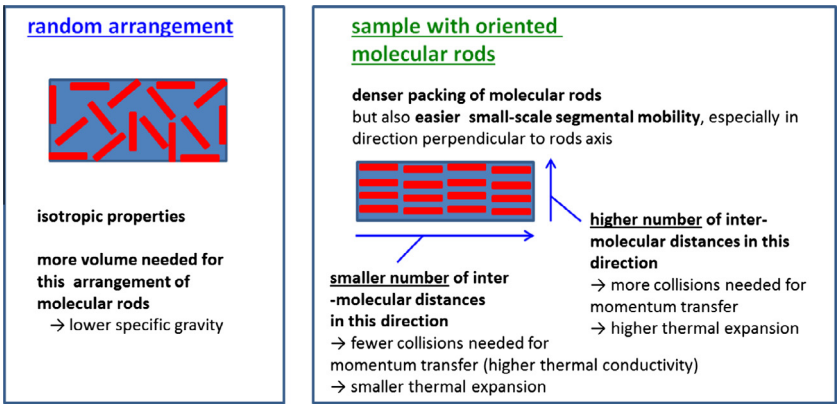

Scheme 2. Effects of orientation of rod-like molecules of a polymer matrix on its selected properties.

In their previous work [3,26–28], the authors have investigated epoxy networks with mesogenic building blocks. In the work [26] they compared the suitability of several mesogen-based epoxy matrices for the orientation in magnetic field and for the enhancement of this orientation by diphenyl aluminium phosphate nanorods ("NR", see Scheme 3). The epoxy matrix based on the mesogenic diepoxide "LCEM" (see Scheme 3) and 4,4′-diaminodiphenylmethane (DDM) was found to display promisingly high degrees of orientation and was hence selected for a detailed study presented in this work, which focusses on a thorough characterisation of the LCEM/DDM/NR system, including its cure and gelation behaviour, its morphology, on the quantitative characterisation of the achieved global orientation, on the influence of the magnetic field direction, as well as on the characterisation of their temperature-dependent dynamic-mechanical properties.

2. Experimental

2.1. Materials

The liquid crystalline diepoxy monomer (LCEM) used in this study is bis[4-(10,11-epoxyundecanoyloxy)benzoate] *p*-phenylene. The synthesis procedure of the LCEM, its structure and characteristics were described in detail elsewhere [27]. As curing agent, a stoichiometric amount of 4,4′-diaminodiphenylmethane (DDM) was used. As anisotropic filler, crystallites of aluminium diphenyl phosphate (NR) were used, which displayed moderately to distinctly elongated cuboid shapes of 400–1200 nm width and 600–2000 nm length (see TEM in Fig. 3). These crystallites are composed of nanorods (formula: $Al[O_2P(OPh)_2]_3$, see Scheme 3) and were synthesized according to the method reported in the literature [29,30]. All the reagents and solvents were commercial products from Sigma–Aldrich, Fluka, or Merck, and were used as received. The chemical structures and thermal characteristics of the employed materials are shown in the Scheme 3.

2.2. Preparation of the liquid crystalline resins

The epoxy monomer LCEM was cured in a polyaddition reaction with a stoichiometric amount of the primary diamine DDM, thus yielding the resin depicted in Scheme 4. It can be noted (see Scheme 4) that a layered structure is practically enforced in the ordered domains by the bonding possibilities of the epoxy matrix components LCEM and DDM (see Scheme 3). Additionally, LCEM/DDM composites with 3 wt% of the NR nanofiller were also cured in an analogous way like the neat resin. In the first step of the synthesis procedure, homogenised but uncured "precursor resins" were prepared in 1 g batches as follows: 0.880 g (1.23 mmol) LCEM, 0.122 g (0.616 mmol) DDM and eventually – in case of the composites – 0.031 g NR were put together and homogenised by dissolving (the insoluble NR was finely dispersed) the mixture of the powdery reactants in 10 mL of acetone. In case of LCEM/DDM samples, the mixture was stirred for 5 min, while in case of the LCEM/DDM/NR composites, the stirring was followed by additional sonication for 30 min at room temperature. Finally, the solvent was evaporated under vacuum at room temperature, and the so-prepared mixtures were stored at 5–10 °C before their cure.

In the second and final step of the preparation procedure, the cure of 120-mg-samples was carried out in Teflon moulds (7 mm × 7 mm × 2 mm). The samples were cured at 160 °C for 4 h, followed by post-cure at 180 °C for 2 h. A small oven was used for this purpose, to which a magnetic field of 1.2 T could be applied. The device RTM-1 from REMEL S.C. Nowy Targ, Poland, was used for producing a homogeneous magnetic field in the small oven volume. Samples were cured in two orientations – the lines of the magnetic field were either perpendicular or parallel to the largest surface of the samples, as shown in Scheme 5. After the cure, the samples were allowed to cool below their glass transition temperature with the magnetic field still applied.

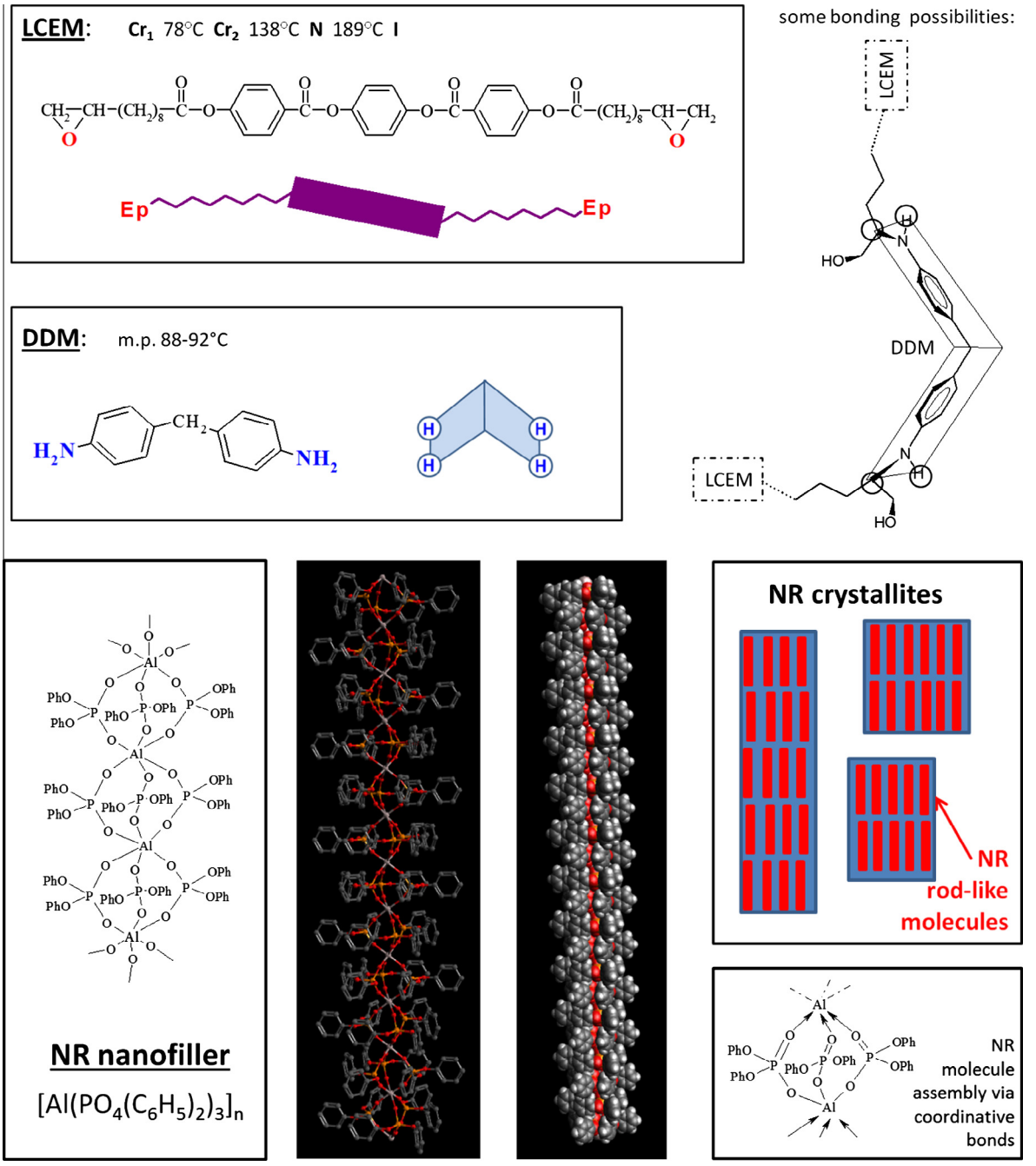

Scheme 3. Components of the liquid crystalline matrix and the tested nanofiller.

2.3. Characterisation

DSC: The crosslinking behaviour and the thermal properties of cured samples were studied using the differential scanning calorimeter DSC822^e from Mettler Toledo. The measurements were performed at the heating rate of 5 or 10 K/min and under nitrogen atmosphere at a flow rate of 50 mL/min.

Infrared spectra, recorded on a Nicolet 8700 (Thermo Scientific) FTIR spectrometer by the ATR technique, were used to investigate the conversion degree of epoxy groups in the cured samples.

Rheological characterisation of the cure reaction was carried out using a HAAKE RheoStress™ 6000 rotational rheometer from Thermo Scientific with parallel plate geometry (aluminium plates, diameter: 25 mm). The plates were preheated to

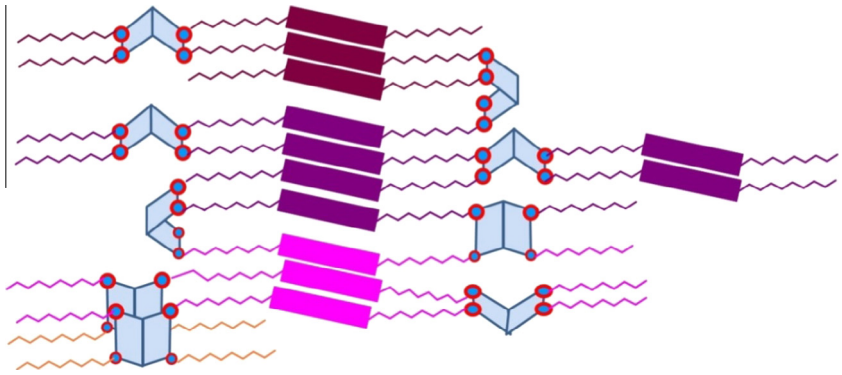

Scheme 4. Idealised structure of the crosslinked matrix: different colors of the LCEM building block symbolize different layers of the crosslinked 3D structure. (For interpretation of the references to colour in this figure legend, the reader is referred to the web version of this article.)

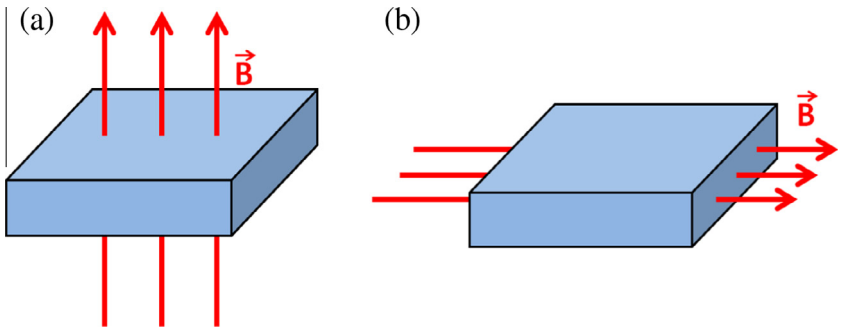

Scheme 5. Vertical (a) and horizontal (b) direction of the magnetic field during cure of samples in Teflon moulds.

the cure temperature. Approximately 0.4 g of the reaction mixture was placed on the bottom plate, and then the top plate was lowered to a gap of ca. 1 mm. Isothermal oscillatory experiments were carried out at 160 °C at a frequency of 1 Hz.

Dynamic-mechanical thermal analysis of the products (rectangular platelets sized 7 × 7 × 2 mm) was carried out on an ARES G2 apparatus from TA Instruments. An oscillatory shear deformation (0.1%) at the constant frequency of 1 Hz and at the heating rate of 3 °C/min was applied, and the temperature dependences of the storage shear modulus and of the loss factor (*G′* and *tan*(*delta*), respectively) were recorded. The temperature range was typically from 25 to +150 °C. The geometry of the deformed area of all the tested samples was always almost the same: 2.5 mm height, 7 mm width, and 2 mm thickness (at top and bottom, 2.25 mm portions of the platelets were inserted into clamps, for sample fixation).

The morphology of the nanocomposite samples was analysed by Transmission electron microscopy (TEM) and was performed using the Tecnai G2 Spirit Twin 12 microscope (FEI, Czech Republic) after preparing ultra-thin sections (approximately 60 nm thick) from the prepared resin platelets by an ultramicrotome (Ultracut UCT, Leica, Germany) under cryogenic conditions (the sample and knife temperatures were −80 and −50 °C, respectively). Each specimen section was transferred to a microscopic grid and observed in the bright field mode at the acceleration voltage of 120 kV.

WAXS/SAXS scattering experiments were performed with samples as they were obtained from the mould (rectangular platelets sized 7 × 7 × 2 mm), and which were fixed with scotch tape on a steel multi-sample-holder with circular windows (5 mm diameters). WAXS/SAXS profiles of the neat mesogen, of DDM and of the nanofiller were measured by fixing finely powdered samples on a scotch tape, the scattering pattern of which was subsequently subtracted from the result. The experiments were performed using a small and (near) wide angle X-ray scattering (SWAXS) camera Molmet (now Rigaku) attached to a microfocused X-ray beam generator (Osmic MicroMax 002) operating at 45 kV and 0.66 mA (30 W), using the wavelength $\lambda = 0.154$ nm. The scattering vector region $q = 0.05–10\ nm^{-1}$ (corresponding to scattering angles $2\theta = 0.07°–14°$; $q = (4\pi/\lambda)\sin(\theta)$, where λ = X-ray wavelength) was probed by means of a 2D electronic wire (Gabriel type) detector with 200 mm diameter. It was used in two distances: either 2200 or 400 mm from the studied sample. At larger angles in the near-WAXS region of $q = 4–40\ nm^{-1}$ ($2\theta = 5.6°–58.7°$), an imaging plate (IP) from Fujifilm was used to detect the scattering intensity in dependence of q (angle), which was subsequently digitalized (and depicted only in 1D). *Calibration*: For the calibration of the scattering vector in the range $q = 0.05–10\ nm^{-1}$, silver behenate was employed, while powdered silicon was used as calibrator for the near-WAXS range ($q = 4–40\ nm^{-1}$). The scattering intensities were calibrated using a glassy carbon standard.

Orientation Analysis (2D X-ray diffractograms): Oriented samples were studied in the near-WAXS region (q = 4–30 nm^{-1}) with the help of imaging plates. The digitalized data were analysed in 2D form (recalculated from *Intensity* = f(*x, y* coordinates) and to *Intensity* = f(*q*, *azimuth angle*) and some characteristics describing the orientation were calculated.

3. Results and discussion

3.1. Liquid crystalline resin cure

The cure behaviour of the studied LCEM/DDM and of LCEM/DDM/NR was monitored by DSC, at a heating rate of 5 K/min. The obtained thermograms are shown in Fig. 1.

The course of the thermograms of both resins is similar, which indicates that the addition of NR does not alter significantly the course of the crosslinking reaction. The DSC scans show practically the same transitions: The endothermic peaks correspond to the polymorphic transition from crystal$_1$ to crystal$_2$ of the LCEM epoxide (near 80 °C) and to the melting of the DDM curing agent (near 90 °C). The exothermic effect which accompanies the crosslinking reaction appears in direct coincidence with the melting of the LCEM to the liquid crystalline nematic phase above 130 °C. Because of the nearly identical behaviour, both resin compositions (with and without NR) were cured using the same temperature program when platelet-shaped resin specimens were prepared. The *T*-program was developed previously for related LC-epoxy/DDM resins [27,28] and consisted of two stages: In the first step, the sample was heated for 4 h at 160 °C, followed by post-cure for 2 h at 180 °C. The resins were cured both in the absence and in the presence of a 1.2 T homogeneous magnetic field, thus yielding unoriented and oriented specimens, respectively. Generally, the cure program was designed in order to carry out the polyaddition reaction in the temperature range of a nematic phase ($T_{Isotropic}$(LCEM) = 189 °C) of the reaction mixture, thus assuring a reasonable components' mobility, at which a monodomain ordering could be easily enforced by the magnetic field. Secondly, a relatively fast reaction rate was also sought (see below discussion of conversion and gelation), in order to achieve efficient crosslinking. The formation of nematic-ordered linear polymeric intermediates, which are eventually crosslinked to the final epoxy network via formation of lateral bonds between the chains, can be expected in the case of the studied epoxy matrix, in analogy to earlier observations [2] on similar liquid crystalline epoxy systems. As mentioned above, the bonding possibilities of LCEM and DDM are expected to enforce a layered arrangement of LCEM units in the crosslinked matrix (such an arrangement was indeed observed experimentally, see further below).

The *completeness of the epoxy-amine polyaddition* was evaluated by means of IR spectroscopy: in all samples the peaks characteristic for epoxy groups, observable near 915 and 760 cm^{-1}, disappeared almost completely, which confirmed a highly efficient cure.

In order to study the cure reaction in more detail, parallel plate *rheology experiments* were carried out, which yielded the gel points of the tested compositions. The evolution of complex viscosity, storage modulus (G'), and loss modulus (G'') during the isothermal reaction at 160 °C for both LCEM/DDM and LCEM/DDM/NR is shown in Fig. 2. As can be seen in Fig. 2, both moduli, G' and G'' as well as the complex viscosity start to increase approximately after 20 min of cure time in case of LCEM/DDM (Fig. 2a), and after 30 min in case of LCEM/DDM/NR (Fig. 2b), respectively. The analyses were continued until the gel point, which was determined as the cross-over point of the storage and loss moduli. The time of gelation was 11 min (or 39%) longer for the composition with 3 wt% of nanorods, probably due to some ordering of LCEM mesogenic units induced by the presence of the NR crystallites (see discussion further below), which would lead to a sterically more complicated and hence slower growth of the 3D network.

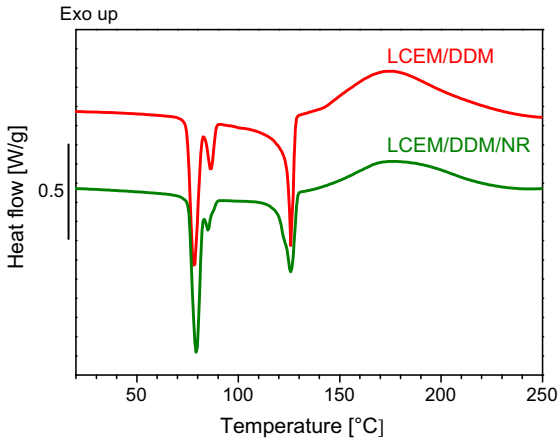

Fig. 1. DSC thermograms of LCEM/DDM and LCEM/DDM/NR compositions; heating rate 5 K/min.

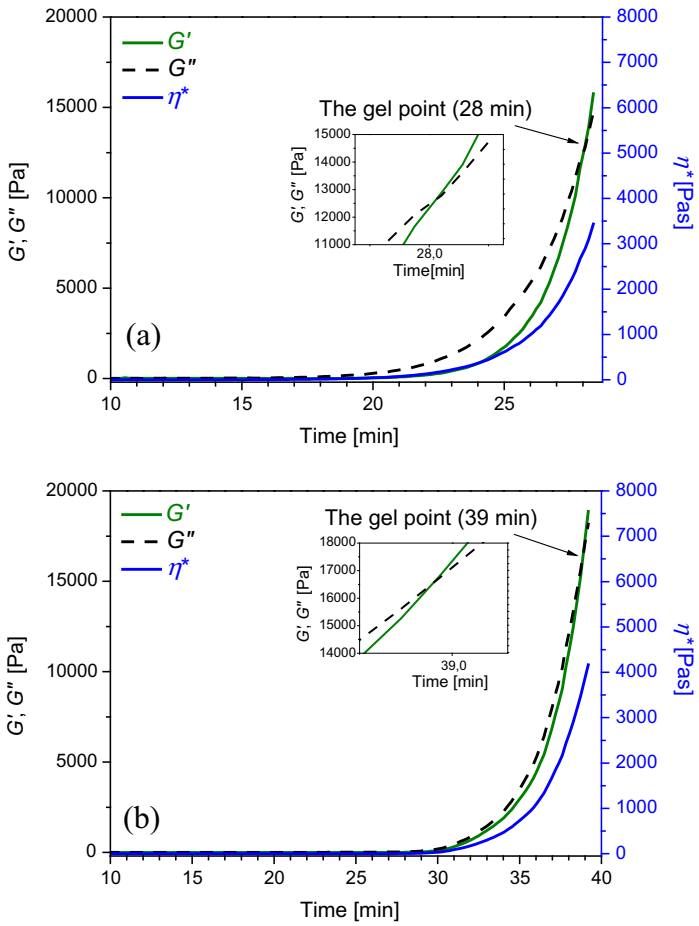

Fig. 2. Evaluation of the complex viscosity (η^*), storage (G') and loss (G'') modulus versus the reaction time at 160 °C for the LCEM/DDM (a) and LCEM/DDM/NR (b) compositions.

3.2. Morphology as observed by TEM

The relatively large NR crystallites, which contain the heavier elements Al and P are well-visible in TEM micrographs of the nanocomposite resins (Fig. 3a–c). It can be observed, that the crystallites approximately preserve the shape of the original (Fig. 3d: size ca. 400–1200 × 600–2000 nm) nanofiller grains, but are up to 20 times smaller (Fig. 3c: ca. 20–60 × 30–100 nm), which indicates splintering of NR crystallites during their dispersion via sonication. The typical NR crystallite shape in the nanocomposite resins is that of a cuboid. They are typically grouped in larger aggregates sized up to several hundred nm, which are probably successors of the original larger crystallites. In case of the nanocomposite LCEM/DDM/NR resins cured in the magnetic field, the aggregates of NR crystallites display little orientation or elongation (Fig. 3a and b) similarly like in the specimen cured without field (Fig. 3c). However, as will be discussed further below, the individual nano-grains were found to be distinctly oriented when analysed by 2D-X-ray scattering.

It should be noted that the oriented samples in Fig. 3 were cut in the direction of the magnetic field lines, so that an eventual anisotropy in the field direction should be well visible. The small sizes, as well as the nearly cubic nanofiller (NR) shape, are highly favourable for its order-enhancing effect on the matrix. The contact surface is high, and the nearly dot-like nanoparticles much easier can rotate and align along the magnetic field lines in the viscous (see η^* in Fig. 2) matrix, than would do longer needle-like crystals of NR (which could be easily prepared).

An interesting feature is the fibrous surface of (nanofiller-free) uneven break regions in magnetic-field-oriented samples (Fig. 3e). This pattern coincides with the orientation of the rod-like epoxy mesogen molecules (invisible by TEM) of the matrix, which was proven by 2D SAXS/WAXS images (see below).

3.3. Orientation in the liquid crystalline resins (WAXS/SAXS)

The X-ray scattering patterns of the prepared LC resins and nanocomposites and the orientation and ordering effects in them are illustrated in Figs. 4–8. The oriented structure was assigned as smectic C (see below), which confirms the expected

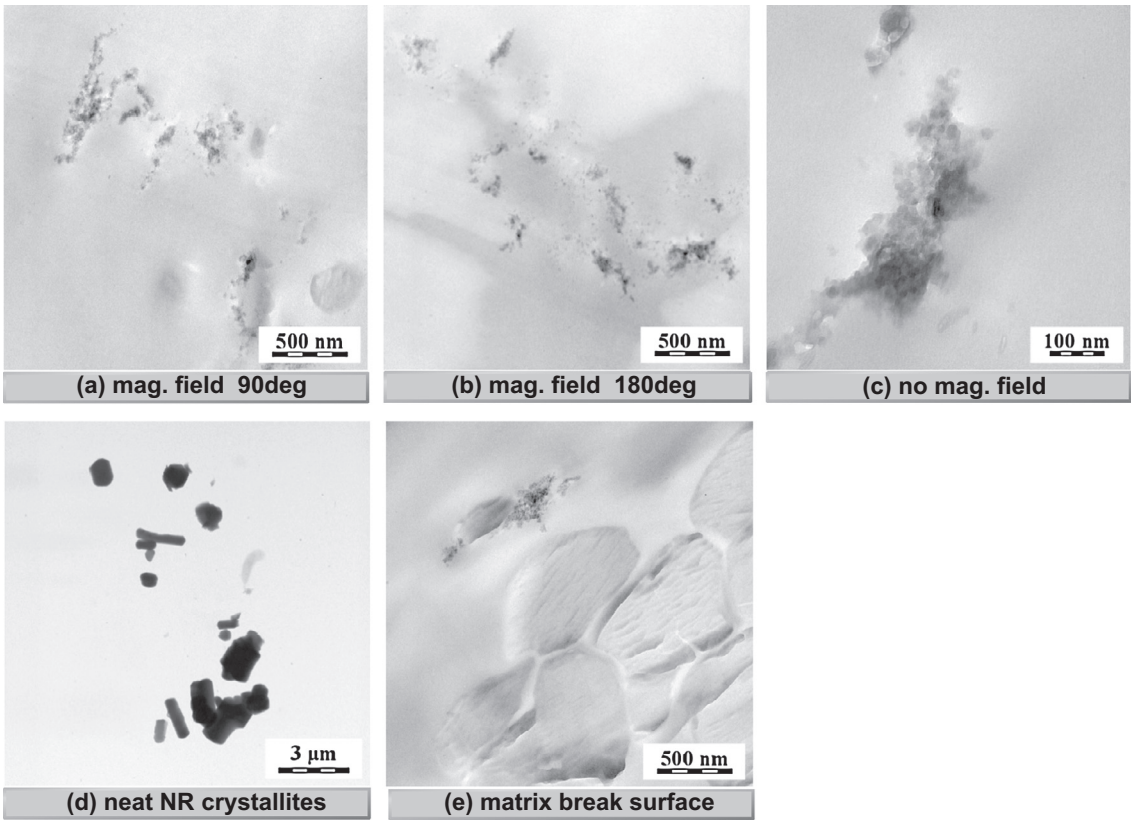

Fig. 3. TEM micrographs of the LCEM/DDM/NR resin cured (a) with magnetic field perpendicular to sample surface (sample cut parallel to field lines), (b) with magnetic field parallel to sample surface (sample cut parallel to field lines), (c) without magnetic field (sample cut perpendicular to main surface; same morphology, but higher image detail than in a, b); TEM micrograms of (d) neat NR crystallites, (e) of the neat matrix break surface.

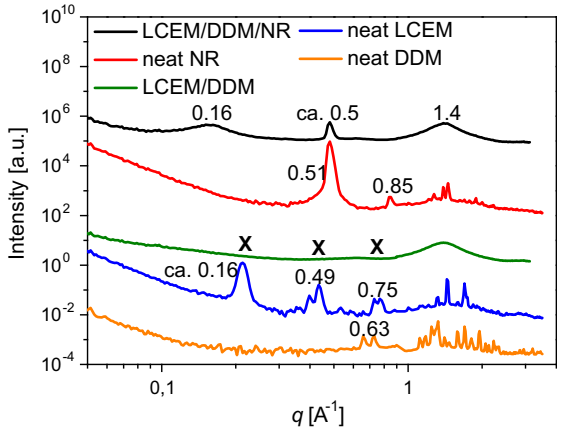

Fig. 4. SAXS/WAXS patterns of LCEM/DDM and LCEM/DDM/NR resins cured without magnetic field, as well as of the neat components LCEM, DDM and NR; the most characteristic interferences are labelled with the scattering vector q values; in case of the LCEM/DDM system, the interferences at q = 0.16, 0.49 and 0.75 are practically invisible in 1D-SAXS/WAXS, but can be observed with high-resolution 2D-SAXS for magnetic-field oriented LCEM/DDM.

arrangement of LCEM units in layers. Generally it was possible to observe, that the presence of the NR nanofiller – which itself also is ordered by the magnetic field – strongly enhances the ordering effect of the magnetic field on the LC epoxy resins. Some spontaneous weak global orientation caused by NR was observed even in absence of the magnetic field. Interesting was also the finding, that the field direction, parallel or perpendicular to the main surface of the platelet-like samples, had a distinct effect on the achieved degree of ordering, which was even more sensitively detected by DSC and dynamic-mechanical thermal analysis.

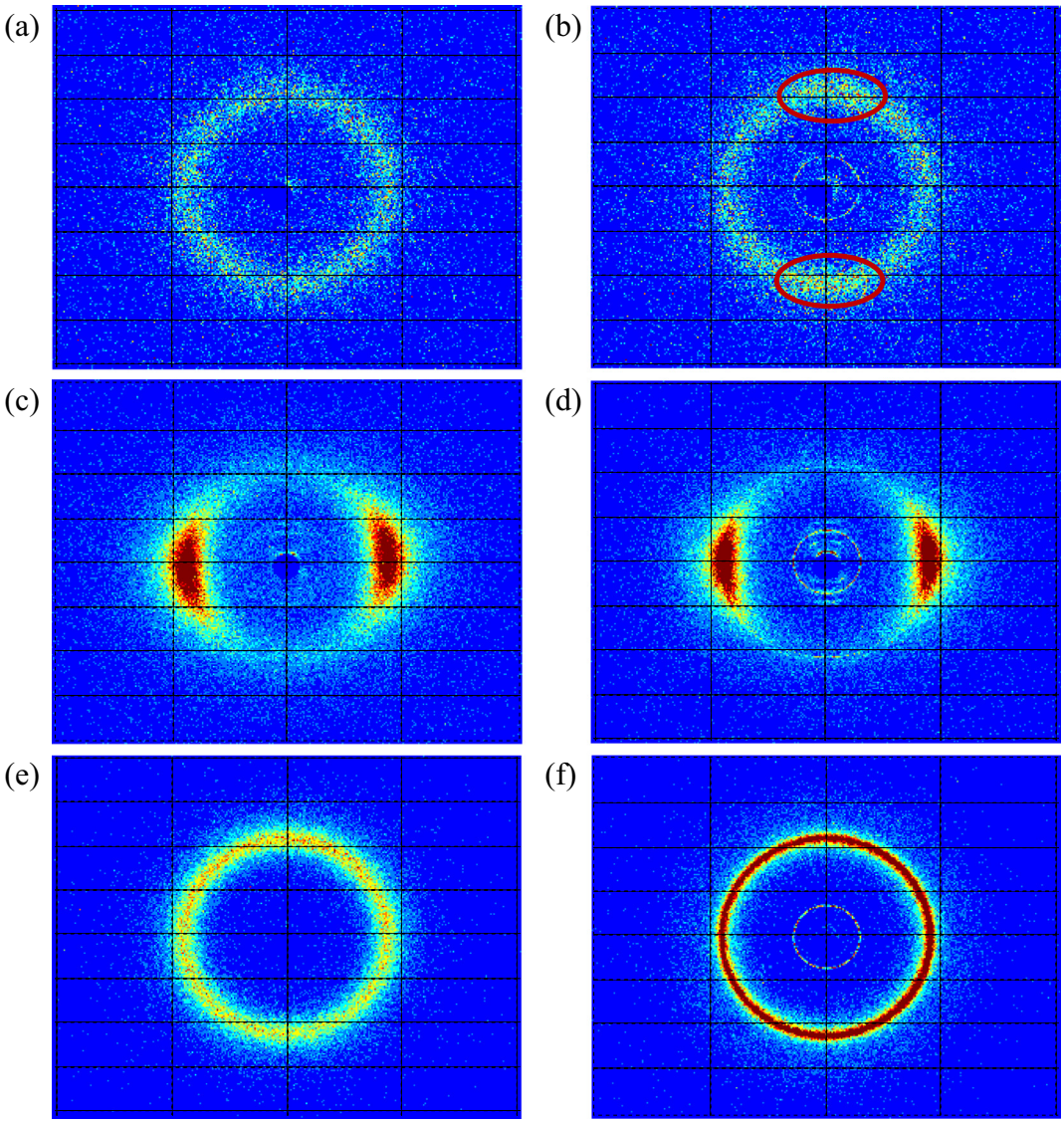

Fig. 5. 2D-WAXS images of the LCEM/DDM (left column: a, c, and e) and LCEM/DDM/NR (right column: b, d, and f) resins, cured without magnetic field (top row: a and b), with in-plane magnetic field of vertical direction (centre row: c and d) or with magnetic field perpendicular to the main sample surface (bottom row: e and f).

3.3.1. Characteristic interference peaks

The X-ray scattering patterns of the prepared resins (1D-WAXS/SAXS in Fig. 4 and 2D-WAXS/SAXS in Figs. 5 and 6a) display the following interference maxima, which can be correlated with the structural features of their components: *LCEM*: $q = 1.4$ Å^{-1} (intense and somewhat broad; corresponds to $d = 4.4$ Å which can be assigned to the lateral distance of LCEM rods), $q = 0.75$ Å^{-1} (weak, $d = 8.4$ Å), $q = 0.49$ Å^{-1} (weak, $d = 13$ Å, corresponds to the width of the aromatic core), 0.32 Å^{-1} (weak, second order maximum of the reflection at $q = 0.16$ Å^{-1}), $q = 0.16$ Å^{-1} (intense, $d = 39$ Å, corresponds approximately to the LCEM length); *DDM*: $q = 0.63$ Å^{-1} (weak, $d = 10$ Å, corresponds approximately to the length of DDM, not prominent in 2D-SAXS), non-characteristic reflections in the range 1.0–2.0 Å^{-1}; *NR*: $q = 0.51$ Å^{-1} ($d = 12.3$ Å; distance between arrays of electron-rich P and Al atoms in the cores of the NR molecules, as assigned in [30] and verified by comparing homologues with different substituents on NR surface in [30] vs. [29]; in the studied case, $d = 12.3$ Å is also similar to the width of the entire NR molecule), three maxima between $q = 1.3$ and 1.5 Å^{-1} (corresponding to regular Al–Al, P–P and other atoms distances along the main axis of the rod-like NR molecule [30]). The intense reflections at $q = 1.40$ Å^{-1} (LCEM), 0.51 Å^{-1} (NR) and $q = 0.16$ Å^{-1} (LCEM) were investigated with 2D-WAXS and -SAXS (see Scheme 6), in order to assess the orientation of LCEM and NR. The weak reflection of LCEM at $q = 0.75$ Å^{-1} also displays orientation in the 2D-SAXS patterns in Fig. 6a.

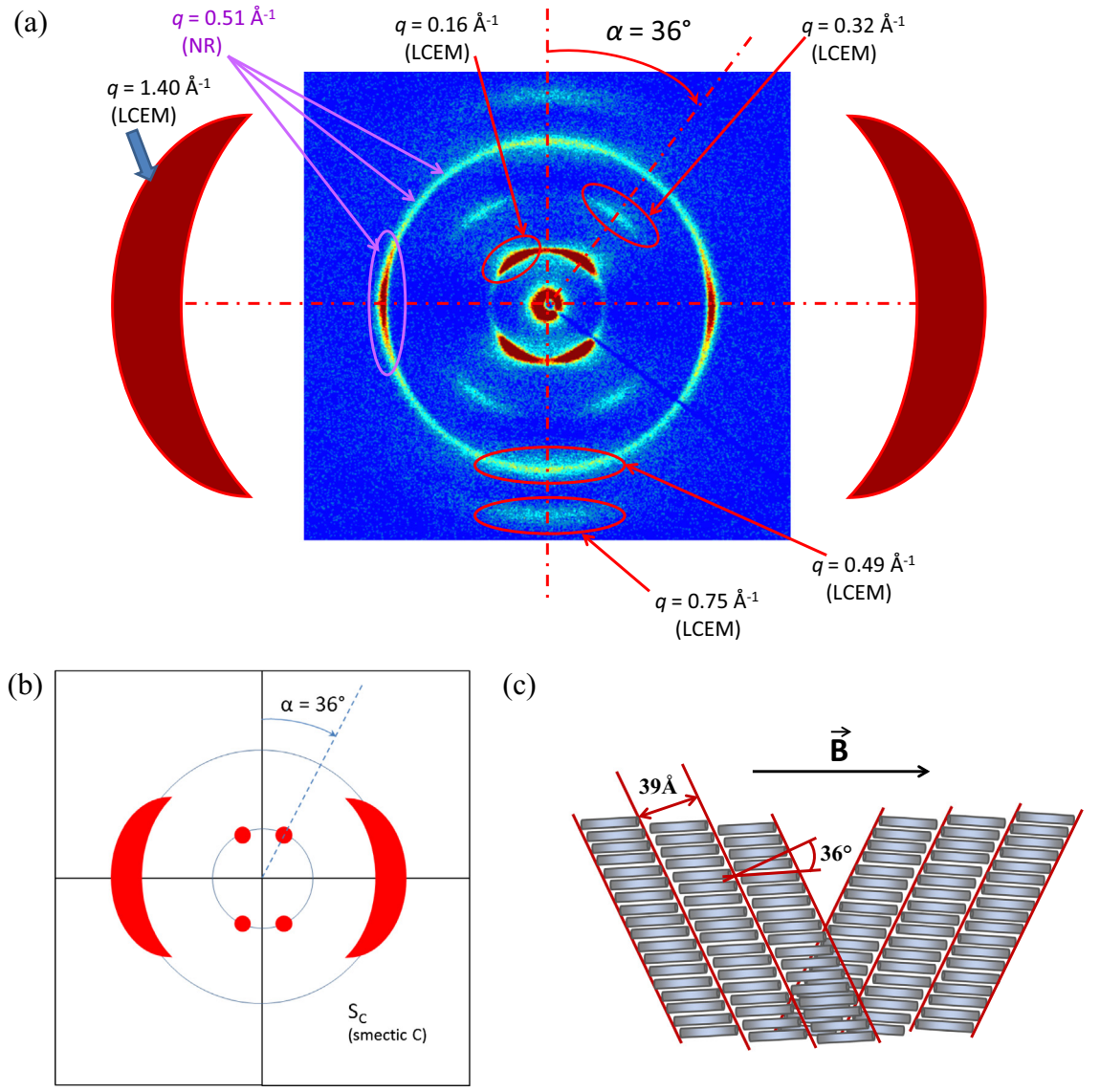

Fig. 6. 2D-SAXS pattern of the LCEM/DDM/NR sample oriented by in-plane magnetic field of vertical direction (a); 2D-SAXS/WAXS pattern expected for the smectic C ordering of rod-like mesogens (b); assigned alignment of the LCEM mesogens in the studied samples (c).

3.3.2. Orientation evaluated by 2D-SAXS/WAXS

In case of the LCEM/DDM resin, no orientation is observed after cure in the absence of magnetic field (see 2D-diffractogram in Fig. 5a), while the sample cured at 1.2 T displays a distinct orientation in the field direction (Fig. 5c and Scheme 6). The scattering intensity in dependence of the azimuth angle for the scattering rings shown in Fig. 5 is evaluated in Fig. 7. From the azimuth plot, the orientation function $orfct = (180 - hw)/180$ can be calculated (where hw is the peak width in degrees in Fig. 5 at half maximum value of the peak intensity). The results of this evaluation are listed in Table 1.

Fig. 6a shows the high resolution 2D-SAXS pattern of the oriented composite resin LCEM/DDM/NR, which is nearly identical with the pattern of the oriented LCEM/DDM matrix (not shown), except for the presence of the narrow and intense ring of the NR interference at $q = 0.51$ Å^{-1} in LCEM/DDM/NR, which overlaps with the interference of LCEM at $q = 0.49$ Å^{-1}.

The interference maxima corresponding to the length and width of LCEM, namely those at $q = 1.40$ and 0.16 Å^{-1}, display a pattern (see Figs. 5c and d and 6a) characteristic of the smectic C structure (see Fig. 6b). The analysis of similar or related structures is discussed in literature, e.g. in [31,32], respectively. The assigned arrangement of the mesogens in lamellae is illustrated in Fig. 6c. The tilted arrangement of the LCEM units in the layered structure of the matrix (Fig. 6c) seems to have its origin in the shape of the LCEM molecule which is shown in Scheme 3: both epoxy-group-carrying linear alkyl chains are attached at an angle to the rigid-rod-like triaromatic core of LCEM.

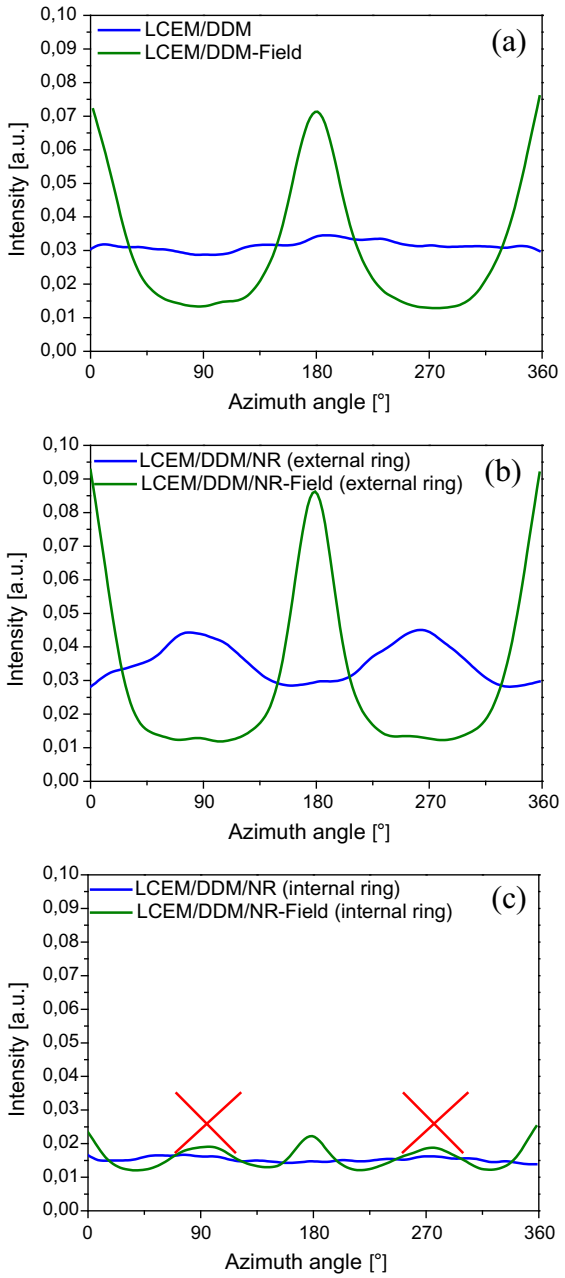

Fig. 7. Evaluation of the orientation from the 2D-WAXS images depicted further above: Intensity in dependence of the azimuth angle for the observed diffraction rings: (a) LCEM/DDM resin cured without magnetic field (blue line) and with magnetic field (green line), ring corresponding to the diffraction at $q = 1.40$ Å^{-1} (related to LCEM); (b) LCEM/DDM/NR resin cured without magnetic field (blue line) and with magnetic field (green line), ring corresponding to the diffraction at $q = 1.40$ Å^{-1} (outer ring); (c) LCEM/DDM/NR resin cured without magnetic field (blue line) and with magnetic field (green line), ring corresponding to the diffraction at $q = 0.51$ Å^{-1} (inner ring, related to NR; the maxima related to the LCEM signal at $q = 0.49$ Å^{-1} are barred with "X"). (For interpretation of the references to colour in this figure legend, the reader is referred to the web version of this article.)

In case of the LCEM/DDM resin oriented with magnetic field parallel to the sample's surface, the *orfct* value of 0.91 is obtained for the reflection at $q = 0.16$ Å^{-1} (four orientation maxima, similar to 2D-SAXS image in Fig. 6) and 0.75 for $q = 1.40$ Å^{-1}.

In case of the LCEM/DDM/NR resin, a weak orientation (Table 1) is observed already in absence of the magnetic field (probable epitaxy effect of the nanofiller), both for the matrix reflex at $q = 1.4$ Å^{-1} (orientation function value: 0.60), as well as for the nanofiller reflex at $q = 0.51$ Å^{-1}. In analogy to the neat matrix, the orientation strongly increases after cure at 1.2 T, with orientation function values of 0.80 (1.4 Å^{-1} signal of LCEM), 0.86 (NR signal at 0.51 Å^{-1}) and 0.89 (0.16 Å^{-1} signal of

LCEM, four 2D-SAXS maxima, shown in detail in Fig. 6a) and with much higher relative intensities of the peaks in the azimuth angle plots (see Fig. 7b).

The nanofiller (NR) reflex at $q = 0.51$ Å^{-1} displays a distinct orientation (0.86) parallel to the magnetic field. The oriented signals of the matrix (LCEM) at $q = 0.49$ Å^{-1}, which are clearly observed if NR is absent, overlap the plot of the NR signals in Fig. 7c and are marked with red "X" in the figure. The cuboid NR nano-crystals hence show a distinct orientation, in which the rod-like constituent molecules are aligned parallel to the magnetic field, although a significant part of NR remains unoriented (ring in Fig. 6a and high baseline in Fig. 7c). This alignment most likely could be driven by the anisotropy of magnetic susceptibility of NR molecules (see also [23]).

3.3.3. Introduction of a 'weighed orientation function'

The above-discussed and widely used orientation function *orfct* is sensitive only to peak width in the azimuth angle plots (Fig. 7), but not to peak height. In order to take into account also the intensity of the orientation peaks (relatively to baseline level), two magnitudes were introduced in the Table 1: *'prominence factor'* = $(I_{max} - I_{min})/I_{max}$ and the *'weighed orfct'* = *prominence factor* $*$ *orfct*, where I_{max} and I_{min} are the maximum and the minimum intensities in the azimuth angle plot (the *prominence factor* is equal to one if the baseline intensity is zero, and approaches zero if the 'peak elevation' $I_{max} - I_{min}$ is small in comparison to baseline intensity). If the so-obtained 'weighed orientation functions' are compared (Table 1), it can be seen, that the orientation effect achieved in the sample LCEM/DDM/NR – FIELD (the magnetic field lines were parallel to the platelet-like sample's main surface) is distinctly higher than in case of the sample LCEM/DDM – FIELD which did not contain the NR filler. In LCEM/DDM/NR – FIELD, the signal related to the length of the LCEM building blocks at $q = 0.16$ Å^{-1} displays a *weighed orfct* value of 0.82, while the signal associated with the lateral distance of the LCEM mesogens at $q = 1.40$ Å^{-1} displays a somewhat lower *weighed orfct* value of 0.69 and hence a lower degree of orientation.

The orientation of NR crystallites parallel to the field in LCEM/DDM/NR – FIELD is less pronounced than the orientation of LCEM, but it is still distinct: a *weighed orfct* value of 0.43 is observed.

The filler-free LCEM/DDM – FIELD sample displays significantly lower *weighed orfct* values for the characteristic reflections at $q = 0.16$ Å^{-1} (*weighed orfct* = 0.79): and $q = 1.40$ Å^{-1} (*weighed orfct* = 0.62). Also the weak LCEM reflection at $q = 0.49$ Å^{-1} displays a higher orientation in the sample with NR filler (see Table 1). Hence it can be concluded, that the NR nanofiller strongly enhances the ordering effect of the magnetic field in the studied resins. Possible explanations of this effect could be epitaxy on NR crystallite surface (rod-like NR molecules as directing agent) and/or the anisotropy of magnetic susceptibility of NR molecules, which could influence the close neighbourhood of NR crystallites.

3.3.4. Effect of the field direction relatively to the samples surface

Interesting is the effect of the field direction, parallel or perpendicular to the main surface of the platelet-like samples, on the degree of ordering caused by the magnetic field. In case of the magnetic field oriented perpendicularly to the main sample surface (both LCEM/DDM and LCEM/DDM/NR), no change in azimuth-angle-dependent ring intensity is observed in the 2D WAXS experiments, in which the X-rays follow the same direction like the magnetic field lines (see Fig. 5e and f). But a difference in the sharpness (line width) of interference rings is clearly visible (Fig. 5e vs. a and Fig. 5f vs. b), suggesting an increased orientation.

The strong enhancement of the global orientation through the effect of NR particles in the LCEM/DDM/NR sample cured with "perpendicular field", in comparison with the NR-free sample cured in the same arrangement, can be seen as a very distinct ring sharpening, if the diffractograms in Fig. 5a vs. e or in Fig. 5b vs. f are compared. A quantitative comparison of the achieved ordering by comparing the azimuth angle dependence of ring intensity (e.g. Fig. 5d) with ring narrowing (e.g. Fig. 5f) is not possible, however.

The following theoretical considerations can be of importance concerning the eventual effect of the direction of the ordering magnetic field: According to the theory of magnetism, the effective magnetic field inside a diamagnetic material is weakened, and the resulting value of the magnetic flux density B in the sample only depends on the permeability of the material, and not on the sample's geometry, as given by the equation $B = \mu H$, where H is the magnetic field strength (which is solely determined by the external magnet) and μ the permeability of the sample. An idealised expectation would be, that the direction of the ordering field respectively to the main surface of the flat sample should not have an effect on the resulting orientation of LCEM and NR, as far as the external field would have the same intensity (H). However, the further below discussed results of thermal and dynamic-mechanical thermal analyses reproducibly suggested that the magnetic field direction has some effect on the degree of ordering in the prepared samples, but a direct proof was missing. A deeper insight was sought with the help of further evaluation of X-ray scattering patterns.

Due to the small thickness of the studied samples, it was not practical to cut the ones ordered by perpendicular field in the field lines' direction and to study the so obtained diminutive specimens (main surface ca. 2×2 mm) by 2D-SAXS/WAXS and by azimuth angle plots (like it was done in case of the large $7 \times 7 \times 2$ mm samples ordered by 'parallel field'). Instead, the orientation was evaluated at least qualitatively by comparing peak widths in 1D-SAXS/WAXS patterns. The 1D-SAXS/WAXS curves shown in Fig. 8 correspond to radial cuts (from centre to border) through the images compared in Fig. 5, in which the intensity (value as colour) depends on two coordinates (or, more practically, on radius and on azimuth angle). The SAXS/WAXS patterns in Fig. 8 depict the scattering intensity in dependence of the scattering vector (q), which in turn is calculated

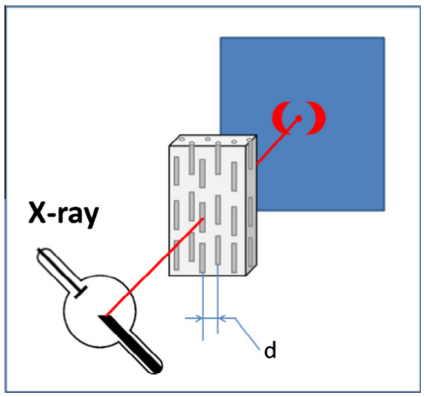

Scheme 6. Orientation in a sample with rod-like blocks and the resulting pattern of 2D-X-ray scattering.

Table 1
Evaluation of the degree of orientation of the liquid crystalline resins prepared: *θmax* is the azimuth angle position of the maximum of a scattering peak, *hw* is the width of the peak in degrees at half-of-maximum-intensity, *orfct* is the orientation function; in case of the samples with the "–FIELD" suffix, the applied magnetic field was always parallel to the samples' main surface.

Sample signal	*θmax* [deg]		*hw* [deg]	*orfct*	Prominence factor	Weighed orfct
LCEM/DDM – FIELD 0.16 $Å^{-1}$, all four LCEM peaks	36, 144	216, 324	16.5	***0.91***	0.87	***0.79***
LCEM/DDM – FIELD 0.49 $Å^{-1}$ (LCEM)	90	270	64	***0.64***	0.26	***0.17***
LCEM/DDM – FIELD 1.40 $Å^{-1}$ (LCEM)	0	180	44.5	***0.75***	0.82	***0.62***
LCEM/DDM/NR – NO FIELD 1.40 $Å^{-1}$ (LCEM)	90	270	72.5	***0.60***	0.37	***0.22***
LCEM/DDM/NR – FIELD 0.16 $Å^{-1}$, all four LCEM peaks	36, 144	216, 324	20	***0.89***	0.92	***0.82***
LCEM/DDM/NR – FIELD 0.49 $Å^{-1}$, LCEM peaks	90	270	51.5	***0.71***	0.37	***0.26***
LCEM/DDM/NR – FIELD 0.51 $Å^{-1}$, NR peaks	0	180	25.7	***0.86***	0.50	***0.43***
LCEM/DDM/NR – FIELD 1.40 $Å^{-1}$ (LCEM)	0	180	36.2	***0.80***	0.87	***0.69***

from the scattering angle (or from the radius in the images in Fig. 5). The changes in the degree of ordering of the LCEM units in the compared samples were evaluated as changes in the shape of the peak at $q = 1.4$ $Å^{-1}$. A broad and flat peak corresponds to an amorphous, non-ordered structure, while a needle-like peak (or a group of such peaks: see patterns of neat resin components in Fig. 4) corresponds to a highly ordered or even crystalline state.

The results in Fig. 8 show the effect of the absence of field, of parallel and of perpendicular field on the ordering of LCEM units in LCEM/DDM (Fig. 8a) and in LCEM/DDM/NR (Fig. 8b). It can be seen, that the difference in ordering between parallel and perpendicular field is invisible by SAXS/WAXS for the neat matrix LCEM/DDM, but the thermal and dynamic-mechanical thermal analyses (see further below) still indicate some difference in the internal properties. In the case of the LCEM/DDM/NR resin, which generally tends to a higher orientation, a distinct increase of orientation (peak narrowing + higher peak intensity) can be observed, if perpendicular magnetic field is applied in place of the parallel one. Distinct differences in thermal and *T*-dependent dynamic-mechanical properties were also observed for this resin.

As confirmation of the above discussed method of evaluation of orientation degree, Fig. 8c and d compares the 1D-SAXS/WAXS patterns for sample sets ordered by parallel and by perpendicular field. For both field directions, the order-enhancing effect of NR (peak narrowing) is distinctly visible. This NR effect was already well-proven by the above discussed 2D-SAXS/WAXS investigations illustrated in Figs. 5 and 7. Also in case of the comparison shown in Fig. 8c and d, it can be observed, that the obviously more efficient perpendicular field causes a stronger ordering effect of NR on the matrix.

The marked effect of the magnetic field direction on the degree of ordering in case of LCEM/DDM/NR contradicts what would be expected according to the simple theory of diamagnetism. The number of LCEM molecules, which are to be aligned in both cure arrangements (with parallel and with perpendicular field) is the same. The nature of the 'field-direction-effect' could not be proven, but a tentative explanation might be suggested: In the case of the perpendicular field, a smaller number (3.5 times) of LCEM molecules (which undergo brownian motion) has to be aligned per one magnetic field line, which would lead to more favourable ordering statistics than in case of a longer alignment paths through the sample.

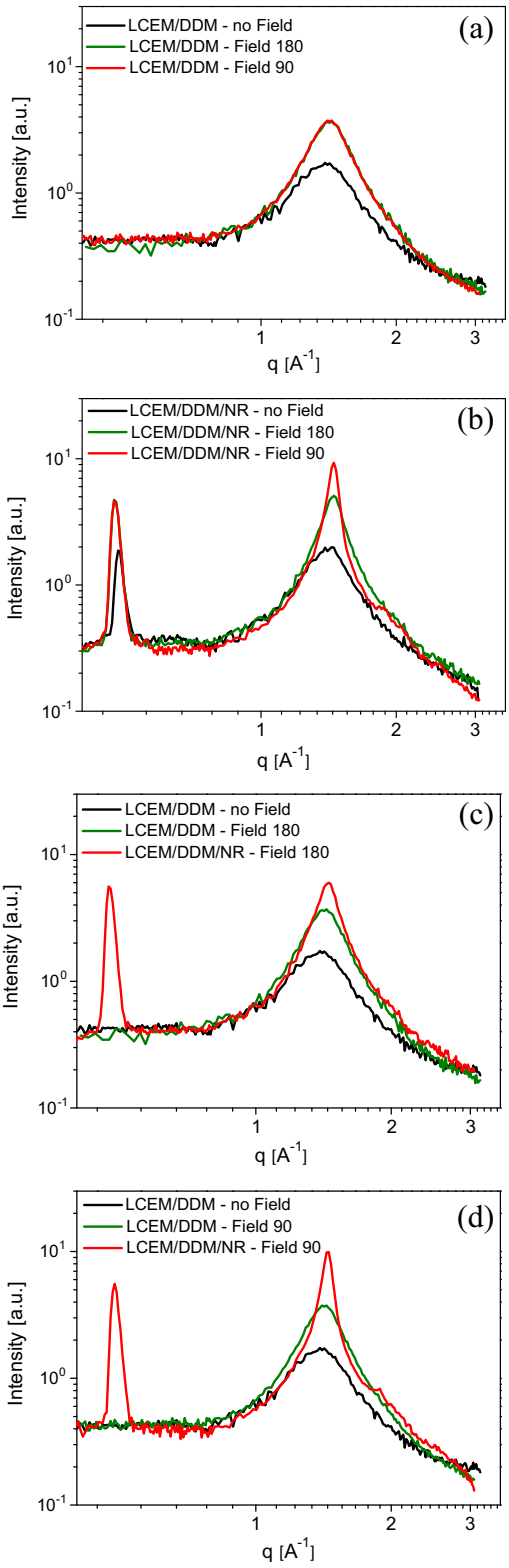

Fig. 8. Degree of ordering of the LCEM units in dependence of the presence and direction of magnetic field during the resins' cure, evaluated qualitatively using the 1D-WAXS/SAXS peak at $q = 1.40$ Å^{-1}: (a) LCEM/DDM resin cured without magnetic field, in a field parallel to the main sample surface ("Field 180") and in a field perpendicular to the surface ("Field 90"); (b) the same comparison for the resin LCEM/DDM/NR which contains the orientation-enhancing nanofiller NR; (c) illustration of the effect of the addition of NR on the degree of ordering for LCEM/DDM cured without field, cured in the "in plane" (180°) field and LCEM/DDM/NR cured in the 180° field; (d) NR effect for LCEM/DDM cured without field, cured in the "perpendicular" (90°) field and LCEM/DDM/NR cured in the 90° field.

3.4. Thermal and dynamic-mechanical properties of the liquid crystalline resins

3.4.1. Differential scanning calorimetry

DSC thermograms of cured LCEM/DDM and LCEM/DDM/NR networks are presented in Fig. 9a and b. Both compositions cured under the 1.2 T magnetic field exhibit slightly lower glass transition temperatures (T_g) than analogous samples crosslinked without the field. These results seem to indicate that the ordering induced by the magnetic field lowers the glass transition temperature of the resins with rod-like mesogen building blocks.

The magnetic field orientation towards the flat samples' main surface was also found to have an influence on the T_g values: For the LCEM/DDM/NR resins, a simple trend of T_g was found: Without magnetic-field-orientation the T_g value was 85.0 °C, with the field parallel to the main surface of the flat sample T_g was 84.0 °C, and with the "perpendicular field" T_g was 81.0 °C. The T_g value was found to decrease with the increasing LCEM ordering which was observed by X-ray scattering (see above). In the case of the neat matrix, LCEM/DDM, the trend was more complex, although the ordered samples generally displayed a lower T_g than the non-ordered one: T_g was 82.5 °C for the non-ordered sample, 81.0 °C for the sample with field parallel to the main surface, and 82.0 °C for the "perpendicular field".

The LCEM/DDM samples oriented with different field direction displayed an identical or very similar degree of orientation according to X-ray scattering, so that the differences in T_g have likely a more complex cause than the degree of orientation alone. The dynamic-mechanical thermal analysis (DMTA, see below) yielded the same (but stronger) trends of T_g values for all the tested resins, like the DSC investigations.

The reason for lower T_g for the samples cured under magnetic field is presumably the higher degree of ordering (observed by X-ray). An easier segmental mobility could be expected for aligned rod-like epoxy building blocks in the matrix, rather than for randomly arranged ones, which would block each other in a strained network (like aligned vs. randomly oriented matches, see also Scheme 2 right vs. left). The flexible chains at the ends of the LCEM structural units should allow both the segmental mobility as well as different arrangements of the epoxy network.

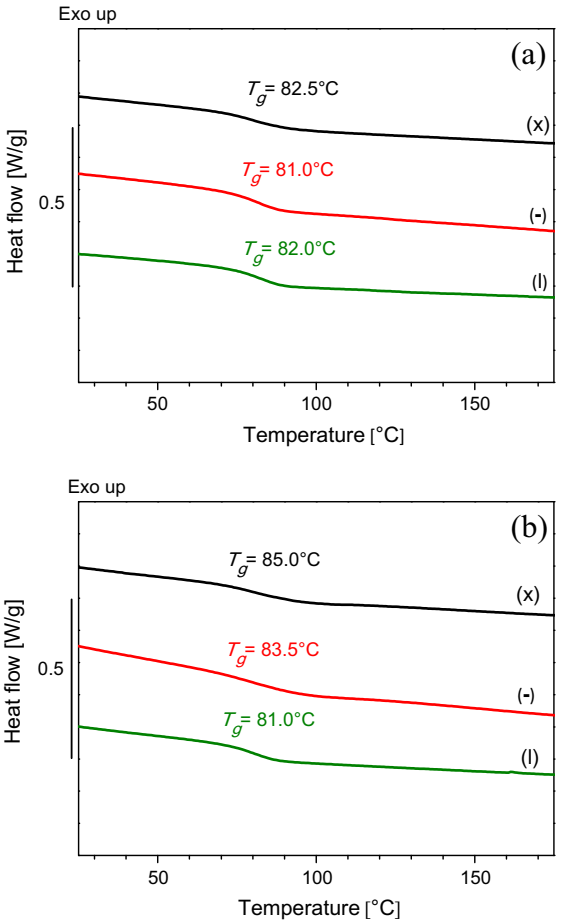

Fig. 9. DSC thermograms of (a) LCEM/DDM and (b) LCEM/DDM/NR compositions cured under magnetic field in vertical (|) and horizontal (–) direction, as well as in absence of magnetic field (×); the heating rate was always 10 K/min.

3.4.2. Dynamic-mechanical thermal analysis (DMTA)

The *T*-dependent dynamic-mechanical properties of the neat LCEM/DDM resin and of LCEM/DDM/NR composites cured with and without magnetic field were also investigated (see DMTA results in Fig. 10) and correlated with their internal orientation established by WAXS/SAXS analyses. The properties of the anisotropic samples cured in the 1.2 T field were analysed in several sample orientations, taking into account the alignment of the ordering direction and of the stress applied during the analysis. Scheme 7 shows the different setups of samples' deformation during DMTA, and highlights the orientation of mesogenic groups in the resins, as determined above by WAXS/SAXS.

In case of the LCEM/DDM resin (see Fig. 10a), the anisotropic samples cured under magnetic field display practically always higher moduli than the sample cured in the absence of magnetic field, especially in the rubber region. In the deformations b and c from Scheme 7, the mesogenic units are either twisted in respect to each other ("twisting"), or shifted in respect to each other along an axis perpendicular to the mesogens' longest dimension ("lateral shifting"). In such deformation modes, the anisotropic LCEM/DDM resin poses the highest resistance to deformation, thus leading to the highest moduli in the rubber region. The "twisting" deformation yields the highest modulus in the glass region and also nearly the highest modulus in the rubber region, where nevertheless the "lateral shifting" leads to a slightly higher resistance. In the deformation d from Scheme 7, the mesogenic LCEM units are shifted along their longitudinal axis in respect to each other ("longitudinal shifting"). This deformation was found to pose the smallest resistance, but still its rubber modulus is higher than in the non-oriented sample.

For the nanocomposite LCEM/DDM/NR resin (see Fig. 10b), the trends in the temperature-dependent moduli are somewhat similar but more complex than in case of LCEM/DDM. The longitudinal shifting deformation poses the distinctly smallest resistance near the glass transition temperature and below it. For this deformation, the glass transition is broader and begins at lower temperatures than the glass transitions of the other deformation modes. The twisting deformation in LCEM/DDM/NR poses a distinctly smaller resistance in the glass region than the lateral shifting deformation (and even than the longitudinal shifting). Similarly like in the non-filled LCEM/DDM resin, the twisting and lateral shifting deformations

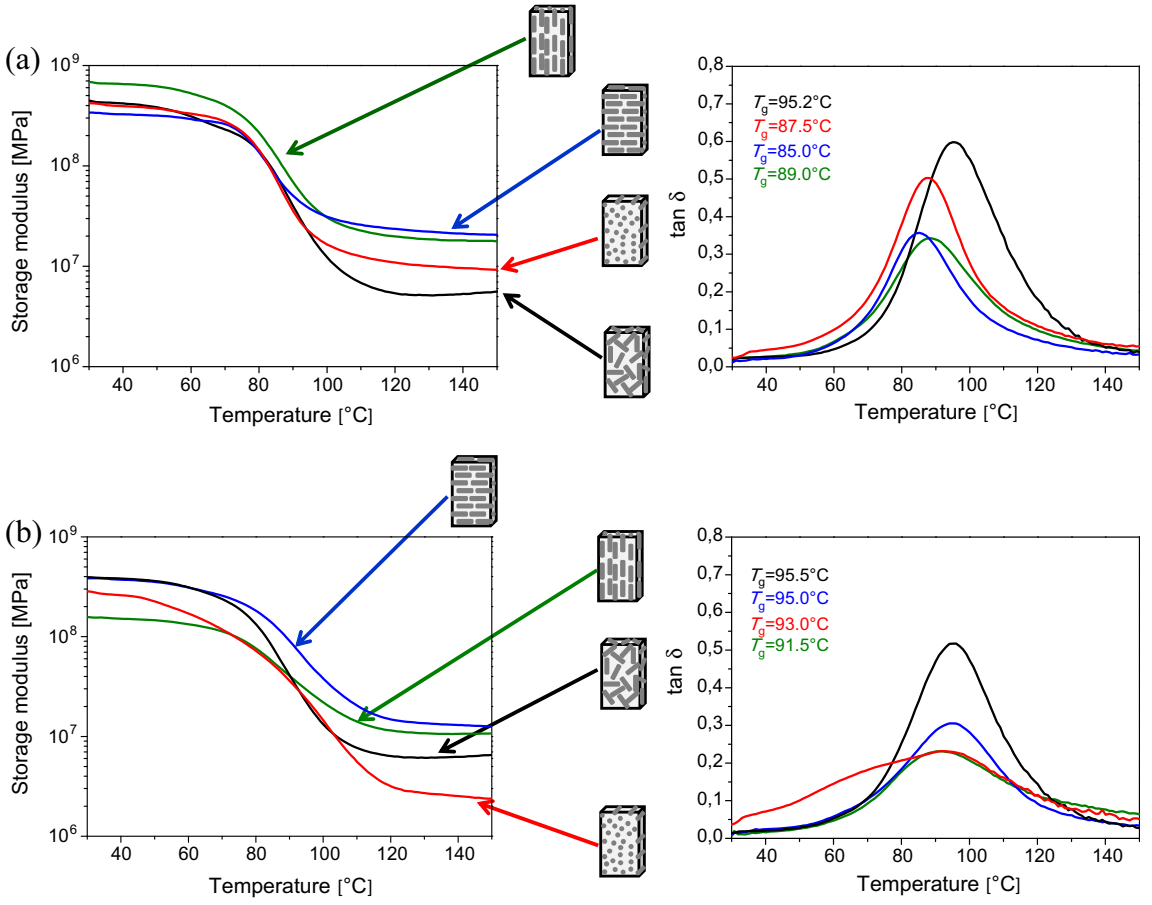

Fig. 10. DMTA thermograms of LCEM/DDM (a) and of LCEM/DDM/NR (b) cured under magnetic field (directions: in-plane vertical, in-plane horizontal, perpendicular to samples' main surface) or without any field; left side of each image: shear storage modulus G′ as function of temperature; right side of each image: loss factor tan(δ) as function of temperature.

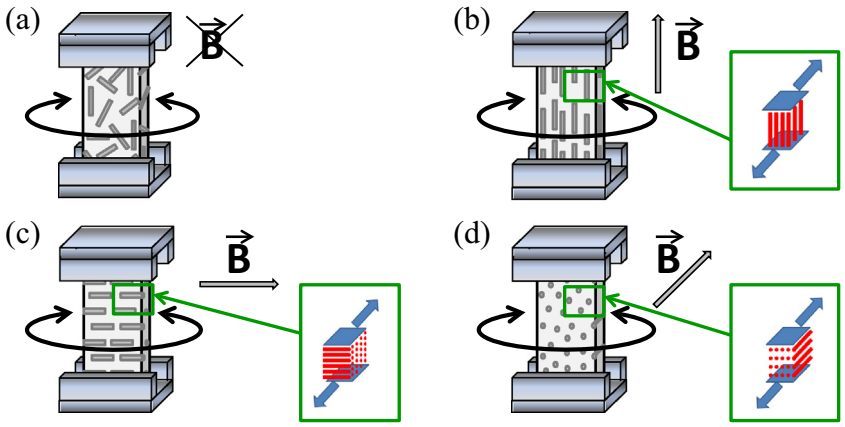

Scheme 7. Different modes of oriented and non-oriented samples' deformation, and the corresponding experimental arrangements during DMTA analysis.

pose a similar resistance in the rubber plateau, but the modulus of the twisting deformation is slightly smaller in this region. In comparison with the filler-free resin, the moduli of the oriented LCEM/DDM/NR resin in all deformation modes are always significantly smaller. In case of the longitudinal shifting deformation, the non-oriented LCEM/DDM/NR resin has a higher modulus in the rubber region than the oriented one. The discussed effects are most likely due to the higher degree of ordering in the LCEM/DDM/NR resins, which is induced by the NR nanofiller. The NR-effect might be the greatest in the case of the sample tested in longitudinal shifting mode, because it was cured with the field perpendicular to its main surface, thus resulting in even higher ordering.

In good agreement with the DSC results, the glass transition temperatures of the resins cured under the magnetic field and without it display analogous trends, although the differences in T_g are rather small in the case of the LCEM/DDM/NR nanocomposite.

4. Conclusions

- Magnetic-field-oriented nanocomposite liquid crystalline epoxy resins were successfully prepared from the rod-like triaromatic polyester oligomer "LCEM", from 4,4′-diamino-diphenylmethane (DDM) and from nano-crystallites consisting of diphenylaluminium phosphate rod-like molecules (NR), by applying a 1.2 T magnetic field during the synthesis.
- It was found (TEM) that the original submicronic crystallites of NR broke up to similar-shaped but much smaller cuboid pieces sized 20–100 nm during their dispersion by sonication. 2D-WAXS investigations of magnetic-field-oriented samples demonstrated a marked orientation of the NR crystallites (not visible in TEM due to cuboid shape), which resulted in NR molecules being preferentially aligned parallel to the field lines. This alignment is probably driven by the anisotropy of magnetic susceptibility of the individual NR molecules.
- The LCEM molecules are markedly oriented by the magnetic field, and the orientation is stronger if the field acts perpendicularly on a thin layer, rather than parallel to the layer.
- The NR nanofiller strongly enhances the magnetic-field-induced orientation of the LCEM units in the curing resin, and this effect is the strongest with perpendicular field orientation. The effect could be connected with epitaxy on the nanofiller surface, due to the rod-like shape of its molecules. The NR crystallites were indeed found to induce some weak spontaneous orientation without any magnetic field. Another contributing factor could be the effect of magnetic susceptibility anisotropy of the NR molecules on their neighbourhood.
- The thermal transition behaviour as investigated by DSC is sensitive to the differences in ordering degree of the resins, even more than X-ray scattering: Lower glass transition temperatures (T_g) are obtained for higher-ordered LCEM/DDM resins.
- The dynamic-mechanical thermal analysis confirms the expected anisotropy of the mechanical properties of the ordered samples (smallest mechanical resistance is found for shearing along the LCEM axis), as well as the decrease T_g with higher degree of ordering.

Acknowledgements

Financial support of Structural Funds in the Operational Programme – Innovative Economy (IE OP) financed from the European Regional Development Fund – Project No POIG.0101.02-00-015/08 is gratefully acknowledged. The authors are indebted to Dr. Krzysztof Lokaj for providing the samples of nanorods.

References

[1] P. Mohan, A critical review: the modification, properties, and applications of epoxy resins, Polym. Plast. Technol. Eng. 52 (2013) 107–125.
[2] C. Carfagna, E. Amendola, M. Giamberini, Liquid crystalline epoxy based thermosetting polymers, Prog. Polym. Sci. 22 (1997) 1607–1647.
[3] B. Mossety-Leszczak, M. Włodarska, Liquid crystallinity in polymers – liquid crystalline epoxy resinsin, in: A. Iwan, E. Schab-Balcerzak (Eds.), Liquid Crystalline Organic Compounds and Polymers as Materials XXI Century: From Synthesis to Applications, Transworld Research Network, Kerala, India, 2011, pp. 125–152.
[4] M. Harada, K. Sumitomo, Y. Nishimoto, M. Ochi, Relationship between fracture toughness and domain size of liquid-crystalline epoxy resins having polydomain structure, J. Polym. Sci. Part B: Polym. Phys. 47 (2009) 156–165.
[5] Ch. Tan, H. Sun, B.M. Fung, B.P. Grady, Properties of liquid crystal epoxy thermosets cured in a magnetic field, Macromolecules 33 (2000) 6249–6254.
[6] Ch. Tan, B.M. Fung, Birefringence and dichroism of oriented epoxy thermoset films, J. Polym. Sci. Part B: Polym. Phys. 39 (2001) 915–919.
[7] Y. Li, M.R. Kessler, Liquid crystalline epoxy resin based on biphenyl mesogen: effect of magnetic field orientation during cure, Polymer 54 (2013) 5741–5746.
[8] D. Ribera, A. Mantecón, A. Serra, Liquid-crystalline thermosets from mesogenic dimeric epoxy resins by tertiary amine catalysis, J. Polym. Sci. Part A: Polym. Chem. 40 (2002) 3916–3926.
[9] E. Amendola, C. Carfagna, M. Giamberini, L. Komitov, Anisotropic liquid crystalline epoxy thermoset, Liq. Cryst. 21 (1996) 317–325.
[10] D.J. Broer, J. Lub, G.N. Mol, Synthesis and photopolymerization of a liquid-crystalline diepoxide, Macromolecules 26 (1993) 1244–1247.
[11] J.Y. Lee, J. Jang, Anisotropically ordered liquid crystalline epoxy network on carbon fiber surface, Polym. Bull. 59 (2007) 261–268.
[12] H. Guo, M. Lu, L. Liang, J. Zheng, Y. Zhang, Y. Li, Z. Li, Ch. Yang, Enhancement in the thermal and dynamic mechanical properties of high performance liquid crystalline epoxy composites through uniaxial orientation of mesogenic on carbon fiber, J. Appl. Polym. Sci. 131 (2014) (online article 40363:1-9).
[13] S.-H. Hsu, M.-C. Wu, S. Chen, C.-M. Chuang, S.-H. Lin, W.-F. Su, Synthesis, morphology and physical properties of multi-walled carbon nanotube/biphenyl liquid crystalline epoxy composites, Carbon 50 (2012) 896–905.
[14] G.G. Barclay, S.G. McNamee, C.K. Ober, K.I. Papathomas, D.W. Wang, The mechanical and magnetic alignment of liquid crystalline epoxy thermosets, J. Polym. Sci. Part A: Polym. Chem. 30 (1992) 1845–1853.
[15] S. Jahromi, Liquid crystalline epoxide thermosets: a deuterium nuclear magnetic resonance study, Macromolecules 27 (1994) 2804–2813.
[16] S. Jahromi, W.A.G. Kuipers, B. Norder, W.J. Mijs, Liquid crystalline epoxide thermosets. Dynamic mechanical and thermal properties, Macromolecules 28 (1995) 2201–2211.
[17] B.A. Rozenberg, L.L. Gur'eva, Ordered liquid-crystalline thermosets, in: A.I. Isayev, T. Kyu, S.Z.D. Cheng (Eds.), Liquid-Crystalline Polymer Systems, Technological Advances, ACS, Washington, DC, 1996, pp. 372–388.
[18] P. Castell, A. Serra, M. Galiá, M. Giamberini, C. Carfagna, Anisotropic thermosets from liquid-crystalline azomethynic epoxy resins and primary aromatic diamines, J. Polym. Sci. Part A: Polym. Chem. 41 (2003) 1–12.
[19] M. Harada, M. Ochi, M. Tobita, T. Kimura, T. Ishigaki, N. Shimoyama, H. Aoki, Thermal-conductivity properties of liquid-crystalline epoxy resin cured under a magnetic field, J. Polym. Sci. Part B: Polym. Phys. 41 (2003) 1739–1743.
[20] M. Harada, M. Ochi, M. Tobita, T. Kimura, T. Ishigaki, N. Shimoyama, H. Aoki, Thermomechanical properties of liquid-crystalline epoxy networks arranged by a magnetic field, J. Polym. Sci. Part B: Polym. Phys. 42 (2004) 758–765.
[21] B.C. Benicewicz, M.E. Smith, J.D. Earls, R.D. Priester Jr., S.M. Setz, R.S. Duran, E.P. Douglas, Magnetic field orientation of liquid crystalline epoxy thermosets, Macromolecules 31 (1998) 4730–4738.
[22] L. Pottié, F. Costa-Torro, M. Tessier, P. Davidson, A. Fradet, Investigation of anisotropic epoxy-amine thermosets synthesised in a magnetic field, Liq. Cryst. 35 (2008) 913–924.
[23] R.S.M. Rikken, R.J.M. Nolte, J.C. Maan, J.C.M. van Hest, D.A. Wilson, P.C.M. Christianen, Manipulation of micro- and nanostructure motion with magnetic fields, Soft Matter 10 (2014) 1295–1308.
[24] Fundamentals of Magnetic Field Effects in M. Yamaguchi, Y. Tanimoto (Eds.), Magneto-Science Magnetic Field Effects on Materials: Fundamentals and Applications, Kodansha Springer, Japan, 2006, pp. 1–40 (Chapter 1).
[25] M. Harada, N. Akamatsu, M. Ochi, M. Tobita, Investigation of fracture mechanism on liquid crystalline epoxy networks arranged by a magnetic field, J. Polym. Sci. Part B: Polym. Phys. 44 (2006) 1406–1412.
[26] B. Mossety-Leszczak, M. Włodarska, Liquid-crystalline epoxy thermosets as matrices for ordered nanocomposites – a summary of experimental studies, Polym. Compos. (2015) 1–9, http://dx.doi.org/10.1002/pc.23585 (published online).
[27] H. Galina, B. Mossety-Leszczak, Liquid-crystalline epoxy resins, J. Appl. Polym. Sci. 105 (2007) 224–228.
[28] B. Mossety-Leszczak, H. Galina, M. Włodarska, U. Szeluga, H. Maciejewski, Anisotropic epoxy networks, Macromol. Symp. 291–292 (2010) 127–136.
[29] Z. Florjańczyk, A. Wolak, M. Dębowski, A. Plichta, J. Ryszkowska, J. Zachara, A. Ostrowski, E. Zawadzak, M. Jurczyk-Kowalska, Organically modified aluminophosphates: transformation of boehmite into nanoparticles and fibers containing aluminodiethylphosphate tectons, Chem. Mater. 19 (2007) 5584–5592.
[30] Z. Florjańczyk, A. Lasota, A. Wolak, J. Zachara, Organically modified aluminum phosphates: synthesis and characterization of model compounds containing diphenyl phosphate ligands, Chem. Mater. 18 (2006) 1995–2003.
[31] S. Dey, D.M. Agra-Kooijman, W. Ren, P.J. McMullan, A.C. Griffin, S. Kumar, Soft elasticity in main chain liquid crystal elastomers, Crystals 3 (2013) 363–390.
[32] C. Tschierske, D.J. Photinos, Biaxial nematic phases, J. Mater. Chem. 20 (2010) 4263–4294.